NO emission prediction using virtual optimized chemistry

Giampaolo Maio[a,*], A. Cuoci[b], B. Fiorina[a]

[a]*Laboratoire EM2C, CNRS, CentraleSupélec, Université Paris-Saclay, 3, rue Joliot Curie, Gif-sur-Yvette 91192, France*

[b]*Department of Chemistry, Materials and Chemical Engineering "G. Natta", Politecnico di Milano, Milano 20133, Italy*

Abstract

A reduced order kinetic model for NO (Nitric Oxide) prediction, based on the recently developed virtual chemistry methodology, is proposed in this article. Temperature and heat release are resolved through the optimization of a virtual main mechanism whereas NO emissions are reproduced through the optimization of a dedicated sub-mechanism. The proposed NO sub-mechanism is optimized over a learning database made of 1D-premixed and 1D opposed jet diffusion flames. The approach is further assessed in a premixed 2D CFD laminar flame computation proposing a direct comparison against fully detailed chemistry.

1. Introduction

Nitrogen oxides (NO_x), emitted in the atmosphere, even in small quantities, cause problems to the local quality of the air contributing to acid rain, ozone production and smog problems.

The numerical prediction of NO_x emission is a challenging task for three main reasons: i) NO_x are produced in very small quantities; ii) NO_x formation and consumption features multiple chemical time scales and iii) NO_x chemical paths vary with the operating conditions (fuel, temperature, pressure, equivalence ratio, etc.).

The complexity of NO chemistry is well illustrated in Fig. 1 which shows the detailed chemistry solution of a stoichiometric and a rich ($\phi = 1.6$) premixed 1-D freely propagating laminar flames. A flame front region zone is first identified in the thermal flame thickness where NO chemistry has a characteristic time scale comparable with the fuel oxidation process. The second zone is the post flame region where temperature as well as all the mayor species are close to their equilibrium value while NO mass fraction evolves at a slow time scale toward its equilibrium concentration.

As observed in Fig. 1 in the post flame NO exhibits two main characteristic behaviours:

- For lean, stoichiometric and moderately rich conditions: A slow NO production until the chemical equilibrium condition is reached Y_{NO}^{eq}. This NO formation is mainly due to the thermal route [1]
- For very rich conditions ($\phi > 1.3$): Slow NO formation and consecutive NO recombination [2] until equilibrium is reached.

The description of NO chemistry in even more challenging if multiple flame regimes are considered (i.e. premixed and non-premixed flames). Indeed in industrial combustion chambers the partial premixing between fuel and air induces mixture stratification at the base of complex combustion regimes development [3].

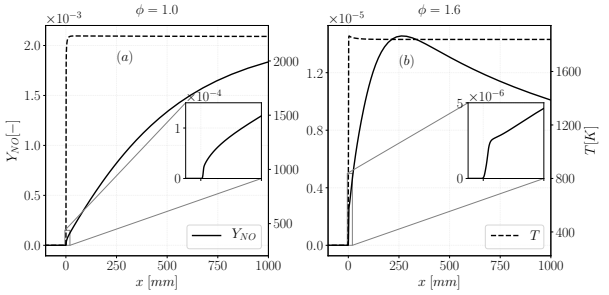

Figure 1: Temperature and NO mass fraction profiles from 1D premixed flames at two different equivalence ratio (stoichiometric and rich) computed with detailed chemistry. The flame front region and post flame one are included in the computational domain. The flame front zone is enlarged in the zoom plots.

Prompt [4], Thermal [1] , Reburning [5, 6], N_2O [2] and NNH [7] NO routes are currently included and combined in the available detailed chemistry databases [8] to describe NO formation in as much as possible flame conditions.

Howhever hydrocarbons detailed chemical mechanisms involve hundreds of species and reactions and their size enormously increases if also NO chemistry is included [9]. Despite the accuracy, the direct inclusion of detailed chemistry in CFD simulations implies an enormous CPU cost. Consequentially reduced order models are needed to attenuate the computational burden [10]. Several reduced models have been developed to account for NO chemistry at low CPU cost [11–15, 15–20].

The recently developed virtual chemistry approach has shown promising capabilities to describe combustion chemistry in mixed combustion regimes at low CPU cost [21], including CO prediction. Virtual chemistry has been also successfully applied in the LES context to predict CO in stratified premixed conditions [22] and including wall heat losses in a confined chamber [23].

*Corresponding author

Email address: giampaolo.maio@centralesupelec.fr (Giampaolo Maio)

The objective of the present study is to propose a new reduced mechanism in the virtual chemistry formalism able to predict NO in mixed combustion regimes. All the NO chemistry pathways included in detailed chemistry are accounted for in the optimization process. In a first step, the mechanism is introduced and validated in 1D flame conditions by comparisons against reference detailed chemistry data. Then, the proposed mechanism is further assessed in a 2D CFD laminar flame simulation employing the open source solver laminarSMOKE [24]. A direct comparison of virtual chemistry computations versus fully detailed chemistry ones is conducted.

2. Virtual scheme architecture

2.1. Principle

Virtual chemistry is a reduced order model for combustion chemistry design to describe pollutant formation [21, 23, 25]. A reduced set of virtual species interact through a reduced number of virtual reactions to reproduce user-defined quantities of interest. As discussed in [21], a virtual chemical scheme is composed of one main mechanism and independent virtual sub-mechanisms. The virtual main mechanism is trained to reproduce the mean mixture properties, temperature, density and heat release rate given by a set of reference database made of an ensemble of flame archetypes computed with detailed chemistry. This main scheme is coupled with the flow solver through the mass, momentum and energy equations. Detailed chemistry ingredients are accounted for during the optimization stage of the main mechanism but, as integrated flame quantities are targeted (flame speed, heat release, etc.), individual species informations are not accessible anymore.

Satellite virtual sub-mechanisms have therefore been introduced to access specific species mass fraction. As an example, a virtual sub-mechanism dedicated to CO prediction have been developed in [21]. The virtual chemistry formalism is presented 2.2 and the main virtual mechanism is briefly remind in section 2.3. A novel virtual scheme architecture dedicated to NO prediction is discussed in section 2.4

2.2. Virtual chemistry theoretical base

A virtual mechanism X includes a N_s virtual species and N_r virtual reactions. A generic reversible virtual reaction R_i^X, which belongs to the virtual mechanism X, is expressed as:

$$\sum_{k=1}^{N_s^i} \alpha_{ki}^{'} \nu_k \leftrightarrow \sum_{k=1}^{N_s^i} \alpha_{ki}^{''} \nu_k \quad i = R_i^X \tag{1}$$

Where N_s^i is the number of virtual species involved in the virtual reaction R_i^X. ν_k denotes the k^{th} virtual species having $\alpha_{ki}^{'}$ and $\alpha_{ki}^{''}$ reactant and product mass stoichiometric coefficients respectively.

The reaction progress q_i for the reaction R_i^X is closed using a finite rate formulation employing modified reaction orders:

$$q_i = k_{fi} \prod_{k=1}^{N_s} [X_k]^{F_k^i} - k_{bi} \prod_{k=1}^{N_s} [X_k]^{B_k^i} \quad i = R_i^X \tag{2}$$

$[X_k]$ is the k^{th} molar species concentration, F_k^i and B_k^i are the forward and backward reaction orders related to the k^{th} species in the i^{th} reaction. k_{fi} and k_{bi} are the forward and backward rate constants. k_{fi} is expressed using an Arrhenius-like formulation:

$$k_{fi} = A_i T^{\beta_i} exp\left(\frac{-E_i}{RT}\right) \quad i = R_i^X \tag{3}$$

A_i is the pre-exponential factor, E_{ai} is the activation energy and in the modified Arrhenius law a temperature exponent β_i is added. When R_i^X is an equilibrated reaction, the backward rate constant is related to the forward one through the equilibrium constant $K_{eq,i}$:

$$k_{bi} = \frac{k_{fi}}{K_{eq,i}} \quad i = R_i^X \tag{4}$$

The kinetic rate parameters of the virtual reactions in the virtual mechanism X are optimized through the evolutionary algorithm proposed by Cailler et *al*. [25].

The optimization problem consists in minimizing the following cost function C:

$$C = f\left(\mathbf{w}^v\left(\chi^v\right), \mathbf{w}^d\left(\chi^d\right)\right) \tag{5}$$

comparing the virtual and detailed chemistry solution through a linear combination of selected normalized flame quantities. χ^v and χ^d are the vector containing the set of thermodynamic, transport and kinetic rate parameters for the virtual and detailed mechanisms respectively. χ vectors allows the calculation of the state vectors $\mathbf{w} = (\rho, u, Y_k, T)$ for virtual ($\mathbf{w}^v$) and detailed chemistry ($\mathbf{w}^d$) through the solutions of the governing balance equation of mass, momentum, species and energy.

χ^d is already known from the detailed thermochemistry and it constitutes an input of the optimization procedure. Whereas χ^v is the the set of free parameters to optimize and consequently is the output of the optimization procedure.

A lower and an upper bound are imposed in the optimization loop, for each parameter of the vector χ^v.

2.3. Main mechanism

The 2-step main virtual mechanism proposed in [25] is retained :

$$\alpha_F^{R_1} F + \alpha_{Ox}^{R_1} Ox \rightarrow I \tag{R_1^T}$$

$$I \rightarrow \sum_{k=1}^{N_P^v} \alpha_{P_k}^{R_2} P_k \tag{R_2^T}$$

The reaction progress of the two irreversible reactions R_1^T and R_2^T are closed with an Arrhenius like formulation as follow:

$$q_1 = A_1 \exp\left(\frac{-E_{a,1}}{RT}\right)[F]^{F_{F,1}}\,[O]^{F_{Ox,1}} \quad (6)$$

$$q_2 = A_2 \exp\left(\frac{-E_{a,2}}{RT}\right)[I]^{F_{I,2}} \quad (7)$$

The pre-exponential constant A_1 and the forward reaction order $F_{I,2}$ are tabulated as function of the fresh gases equivalence ratio. This 2-step structure captures equilibrium flame properties, laminar flame consumption speed and temperature for both lean and rich regimes. The reader may refer to [25] for details and validations cases.

2.4. NO mechanism

A mechanism architecture is proposed to account for all NO chemical pathways discusses in the Introduction and evidenced in Fig. 1. For that purpose, the following NO virtual sub-mechanism, composed of 6 reactions, is proposed:

$$\alpha_F^{R_1} F + \alpha_{Ox}^{R_1} Ox \rightarrow \alpha_{V_1}^{R_1} V_1 + \alpha_{V_2}^{R_1} V_2 + \alpha_{V_3}^{R_1} V_3 \quad (R_1^{NO})$$

$$V_1 + F + Ox \rightarrow \alpha_{NO}^{R_2} NO + \alpha_{V_2}^{R_2} V_2 + F + Ox \quad (R_2^{NO})$$

$$F + NO \rightarrow F + V_2 \quad (R_3^{NO})$$

$$V_3 \rightarrow NO \quad (R_4^{NO})$$

$$V_3 \rightarrow V_2 \quad (R_5^{NO})$$

$$V_2 \leftrightarrow NO \quad (R_6^{NO})$$

where $\alpha_k^{R_i}$ are the mass stoichiometric coefficients associated to species k in the reaction R_i. An ensemble of virtual species V_1, V_2 and V_3 is first produced through the initiation reaction R_1^{NO}. To ensure consistency in fuel (F) and oxidizer (Ox) consumption, the kinetic rate parameters of reaction R_1^{NO} are identical to those of the initiation reaction R_1^T of the main virtual mechanism.

Reactions R_2^{NO} and R_3^{NO} are dedicated to model the fast NO chemistry, which is dominant at the flame front scale. R_3^{NO} is designed to reproduce the fast NO reburning that is mainly important when an excess of hydrocarbon radicals is present in the system [6]. In addition, as it will be shown in sec. 3.2, using two reactions to model fast NO formation, instead of one, enables a better prediction of both premixed and non-premixed flame structures.

Virtual reactions R_4^{NO} to R_6^{NO} describes the NO formation associated to slow chemistry. It includes thermal NO pathway and slow NO reburning phenomena. As discussed later in sec 3.1, this combination of three reactions allows an efficient description of slow NO post-flame formation in both lean and rich regimes. Finally, the equilibrium reaction R_6^{NO} ensures that the chemical equilibrium conditions are well retrieved.

The rate of progress for the reactions set R_1^{NO}-R_6^{NO} are closed using the following Arrhenius-like expressions:

$$q_1 = A_1 \exp\left(\frac{-E_{a,1}}{RT}\right)[F]^{F_{F,1}}\,[O]^{F_{Ox,1}} \quad (8)$$

$$q_2 = A_2 exp\left(\frac{-E_a^2}{RT}\right) T^{\beta_T^2}\,[V_1]^{F_{V_1}^2}\,[F]\,[Ox] \quad (9)$$

$$q_3 = A_3 exp\left(\frac{-E_a^3}{RT}\right)[F]\,[NO]^{F_{NO}^3} \quad (10)$$

$$q_4 = A_4 exp\left(\frac{-E_a^4}{RT}\right)[V_3]^{F_{V_3}^4} \quad (11)$$

$$q_5 = A_5 exp\left(\frac{-E_a^5}{RT}\right)[V_3]^{F_{V_3}^5} \quad (12)$$

$$q_6 = A_6 exp\left(\frac{-E_a^6}{RT}\right)\left([NO]^{F_{NO}^6}\,[V_2]^{F_{V_2}^6} - \frac{[NO]^{B_{NO}^6}\,[V_2]^{B_{V_2}^6}}{K_c^6}\right) \quad (13)$$

The equilibrium constant for the reversible reaction R_6^{NO} is computed as follows:

$$K_c^6 = \frac{[NO]^d\,|^{eq}}{[V_2]^v\,|^{eq}} \quad (14)$$

where $[NO]^d\,|^{eq}$ is a reference NO molar concentration obtained from detailed thermodynamical equilibrium computations. $[V_2]^v\,|^{eq}$ is computed from the knowledge of V_2 mass fraction at equilibrium condition.

Virtual NO sub-mechanisms, although not involved in the closure of mass conservation, is designed according to the hypothesis that:

$$\sum_{k=1}^{N_s^{NO}} Y_k = 1 \quad (15)$$

N_s^{NO} is the the number of species involved in the NO virtual sub-mechanism. Y_{V_3} is equal to zero at equilibrium since the species V_3 is completely consumed through reactions R_4^{NO} and R_5^{NO}. Whereas F, Ox, D and V_1 mass fractions at equilibrium are known quantities at the moment the equilibrium reaction R_6^{NO} is added to the scheme. Consequently Y_{V_2} is computed from Eq. 15.

Reaction orders of reaction R_6^{NO} are constrained by the following equations to ensure a net reaction rate equal to zero at equilibrium:

$$B_{NO}^6 = F_{NO}^6 + 1 \quad (16)$$

$$B_{V_2}^6 = F_{V_2}^6 - 1 \quad (17)$$

The set of kinetic rate parameters to optimize includes the pre-exponential constants A_i the activation energies E_a^i, forward reaction orders F_k^i and species stoichiometric coefficients $\alpha_k^{R_i}$ for reactions R_2^{NO} to R_6^{NO} and the temperature exponent β_T^2. To limit the number of parameters to optimize for F and Ox reaction order are set equal to one. The reactions R_4^{NO} and R_5^{NO} are needed for rich conditions only as will be shown in section 3.1. Consequently the reaction stoichiometric coefficient $\alpha_{V_3}^{R_1}$ is set equal to

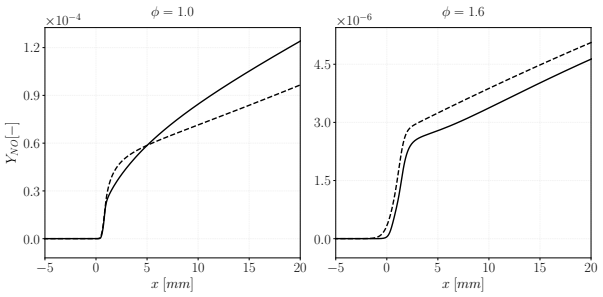

Figure 2: NO mass fraction profiles for stoichiometric (1.0) and rich (1.6) equivalence ratio. Virtual chemistry **VM-6R** NO solution is compared versus the reference detailed chemistry NO. Results are presented at the flame front scale.

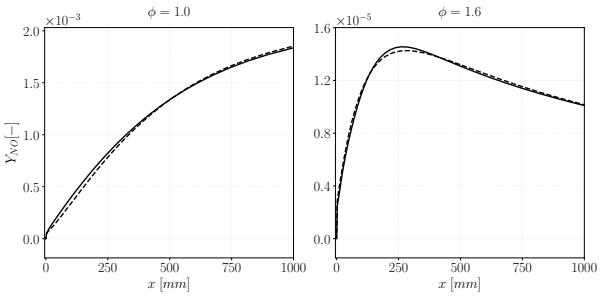

Figure 3: NO mass fraction profiles for a stoichiometric (1.0) and a rich (1.6) equivalence ratio. Virtual chemistry **VM-6R** NO solution is compared versus the reference detailed chemistry NO. Results are presented at the post flame spacial scale.

zero for $\phi < 1.4$. Since the NO mass fraction level is strongly dependent from the equivalence ratio a sub-set of kinetic rate parameters is considered dependent from ϕ. In particular, the pre-exponential constants A_2, A_4, A_5 and A_6 are ϕ-dependent. The kinetic rate parameter of the virtual NO sub-mechanisms are optimized using as reference variable the NO mass fraction of the ensemble of solutions considered in the reference database. NO profiles from 1D premixed laminar flames ($0.5 < \phi < 1.8$) and from non premixed opposed jet flames for several flame strain rates ($a = 50, 150, 300\ s^{-1}$), are retained in the learning database. The reference detailed chemistry profiles are computed for a CH_4/Air mixture using the GRI3.0 mechanism [9]. The optimization procedure is split in two separate steps in which separate reactions block are optimized. Reactions R_1^{NO} to R_3^{NO} are firstly optimized to target the reference NO at the flame front scale. In a second step reactions R_4^{NO} to R_6^{NO} are optimized to predict NO in the post-flame region. At this stage the kinetic parameters of reactions R_1^{NO} to R_3^{NO} issued from the first step are retained. The multi-step optimization process and the target zones definition is not described here because of space limitation.

3. Results: 1D flames

3.1. Premixed flames

The following two mechanism are optimized:

- **VM-6R**: It include the whole set of reactions R_1^{NO} to R_6^{NO}
- **VM-4R**: Reaction R_4^{NO} and R_5^{NO} are removed from the former NO mechanism

The optimized NO virtual mechanisms, are a-posteriori compared versus the reference solutions, for two different equivalence ratios: stoichiometric ($\phi = 1.0$) and rich ($\phi = 1.6$). Results are presented with a spacial scale comparable with the flame front (Fig. 2) and a post-flame spacial scale (Fig. 3) for VM-6R mechanism.

Indeed, the proposed 6-reactions mechanism allows to correctly reproduce Prompt and Thermal post-flame NO formation characterizing lean and stoichiometric conditions. The NO post flame re-burning phenomena encountered in rich flame conditions are also correctly described.

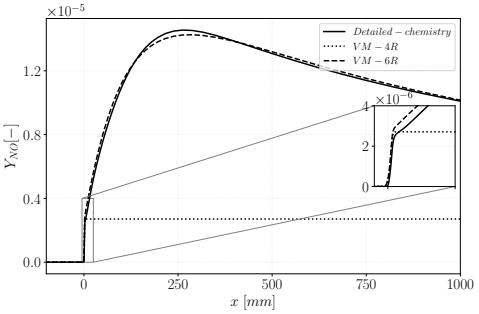

Figure 4: Comparison of NO mass fraction from detailed chemistry and from virtual chemistry considering only 1 reaction in the postflame block (VM-4R) and considering the whole post flame block (VM-6R).

As anticipated earlier in the paper the three reactions R_4^{NO}, R_5^{NO} and R_6^{NO}, that are retained for the post-flame block in rich flame condition, allow to properly retrieve the slow NO consumptions before equilibrium conditions are reached.

A comparison is proposed to stress the importance of retaining reactions R_4^{NO} and R_5^{NO} in the mechanism.

Figure 4 compares, for a rich flame at ($\phi = 1.6$), the results obtained with the two mechanisms (VM-4R and VM-6R) versus the detailed chemistry solution. Indeed by adding the two reactions R_5^{NO} and R_6^{NO} the slow NO formation and recombination processes are properly retrieved, contrarely to the VM-4R case. In stoichiometric conditions the comparison is not shown since the results obtained with VM-6R mechanism and with VM-4R are identical because reactions R_5^{NO} and R_6^{NO} are only activated through $\alpha_{V_3}^{R_1}$ under rich conditions.

3.2. Non-premixed flames

The complete optimized virtual mechanism (VM-6R) is used to a-posteriori compute NO formation in non premixed opposed jet flames.

Figure 5 shows the NO profile computed with the

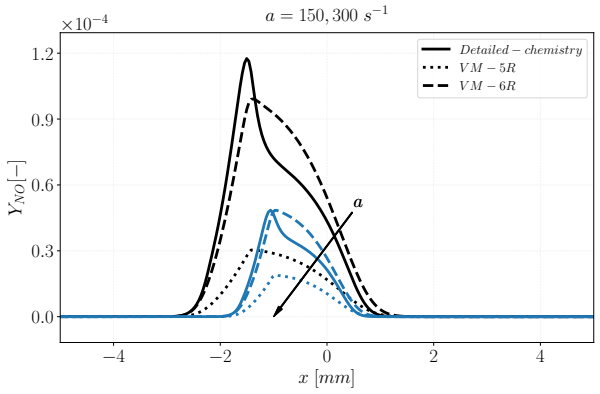

Figure 5: Comparison of NO mass fraction from detailed chemistry and from virtual chemistry considering 1 reaction in the flame front block (VM-5R) and considering the whole post flame block (VM-6R). Different colors are used for different stain rates.

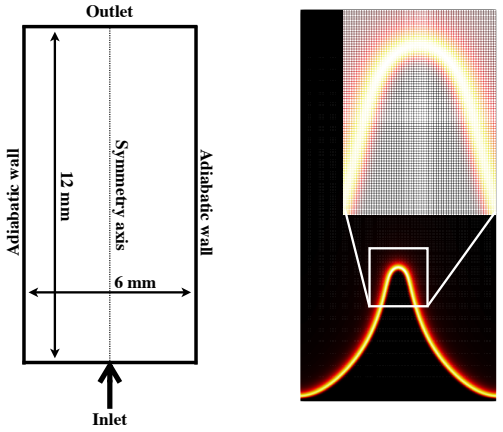

Figure 6: 2D premixed slot burner numerical set-up. On the left schematic view of the computational domain with the corresponding dimensions and the boundary conditions. On the right the normalized heat release rate from numerical simulation shown on the computational grid.

whole proposed mechanism (VM-6R) to the reference profiles for two different flame strain rates.

The proposed virtual NO mechanism optimized in combination on premixed and non-premixed flame archetypes allow to properly retrieve the high sensitivity of the NO profile to the flame strain rate. Indeed increasing the flame strain rate, the flame residence time increases and it impacts on the NO formation.

For comparison purposed, as anticipated above in the article, a test is conducted removing from the mechanism the flame front reaction R_3^{NO} and re-optimizing the whole mechanism. This mechanism is named **VM-5R** in the Fig. 5.

The R_3^{NO} reaction removal does not allow to describe properly the NO profiles in non premixed flame regimes.

The interaction of the carbon chemistry and NO chemistry need at least 2 reactions when both premixed and non premixed flame archetypes are considered in the reference database.

4. 2D slot burner flame

In the current section, 2 dimensional CFD computations are performed employing virtual chemistry and detailed chemistry. The simulation is conducted for a 2D laminar flame benchmark in premixed flame conditions.

The CFD code laminarSMOKE, developed by Cuoci *et al.* [24] is used to perform the computations either for detailed chemistry and for virtual chemistry. LaminarSMOKE is built on the of the open-source suite OpenFOAM [26]. It has already shown capability to accurately model laminar flames including detailed chemistry using hundreds of species and reactions [27, 28]. The transport equations of mass, momentum, energy, and species are solved and the operator-splitting technique [29] is used to timely integrate the species source term [27]. The code laminarSMOKE including also virtual chemistry development is freely distributed [30].

The premixed single slot burner geometry consists in a 2D rectangular computational domain having the size shown in Fig. 6. The boundary conditions include: an inlet, an outlet and adiabatic walls. Since the configuration is axial-symmetric only a half of the computational domain is simulated. The other half of the computational domain is obtained by symmetric reflection of the first part. Therefore a symmetry boundary condition is imposed along the slot axis.

At the inlet a developed laminar parabolic velocity profile is prescribed in the axial direction using a mean value $U_{ref} = 0.6\ m/s$, whereas the others velocity components are set equal to zero.

A uniform squared mesh is considered in the simulation. The characteristic cell size is of about ~ 0.015 mm. This cell dimension allows to fully resolve the thermal thickness and the heat release rate of a premixed laminar flame. In particular, the employed mesh size, ensures 15 to 20 cells across the thermal flame thickness.

A zoom on the computational grid, in the flame tip region, is made in Fig. 6 and an example of normalized heat release rate is also shown on the computational grid. Indeed the heat release rate is properly solved over the employed grid.

Figure 7 shows the temperature and NO field for the 2D premixed burner at stoichiometric conditions. Virtual chemistry results are compared to detailed chemistry ones. Looking to temperature field, it can be noticed that the flame height is correctly captured with virtual chemistry. The NO field is well place in accordance with the temperature one as for detailed chemistry.

A slight underestimation of the NO level is observed. This behaviour is in accordance with the 1D profiles shown in Fig. 2 for stoichiometric conditions.

1-D Temperature and NO mass fraction data are extracted from the 2D field over both axial and a radial directions. The 1D lines used for the comparison are also shown for sake of clarity in the 2D field (Fig.7) in white.

Figure 8 shows the temperature and NO profiles from

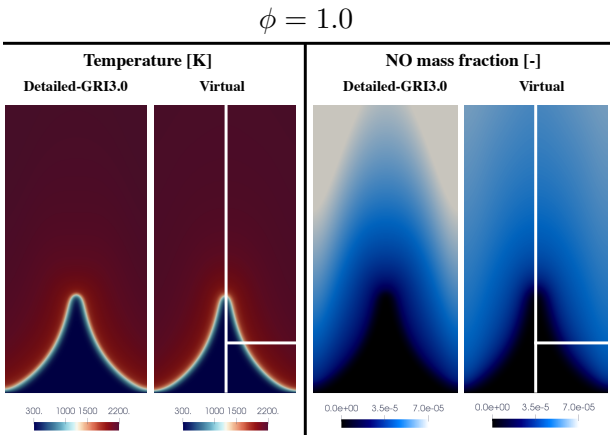

Figure 7: 2D premixed slot burner numerical set-up. Temperature and NO mass fraction colormaps for the 2D laminar slot burner computed with stoichiometric inlet. Virtual chemistry solution is compared with detailed chemistry one.

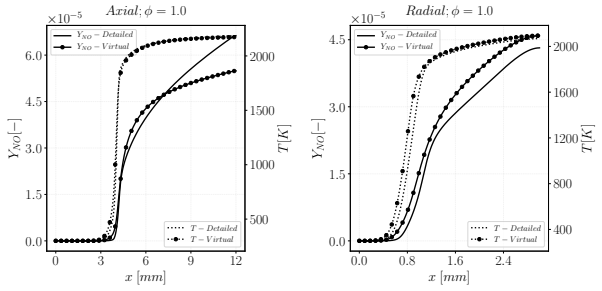

Figure 8: Temperature (dashed lines) and NO mass fraction (solid lines) over both axial (x=0 mm) and radial (y= 2 mm) 1-D lines in the 2-D stoichiometric premixed burner. Virtual chemistry (symbols + lines) is compared against detailed chemistry (lines).

virtual and from detailed chemistry computations along the two lines in the axial and radial direction.

The good temperature accordance in the axial direction confirms that the flame height is well retrieved even if a slight shifting in the radial direction, due to imperfect reproduction of the flame curvature, is observed. NO virtual profiles are consistent with the results obtained in 1-D flame computations shown in Fig.2. The 2D Bunsen flame configuration considered in the present work mainly focuses on the Prompt region and on the first part of the Thermal NO formation.

5. Conclusion and perspectives

NO prediction has been achieved using a reduced set of virtual species and reactions. The proposed virtual chemistry model is able to describe all the NO chemistry pathways that are included in detailed chemistry. In particular Prompt NO, Thermal NO and post flame NO reburning are correctly described by the virtual chemistry model. The developed NO virtual mechanism coupled with the main temperature mechanism is further validated versus detailed chemistry in a 2D laminar premixed Bunsen flame computation. 2D computations of diffusion and partially premixed laminar flame configurations are in progress and will be shown in future works.

References

[1] Y. B. Zeldovich, Selected Works of Yakov Borisovich Zeldovich, Volume I: Chemical Physics and Hydrodynamics, volume 140, Princeton University Press, 2014.

[2] K. K. Kuo, Principles of combustion, TJ254. 5 K85 2005, 2005.

[3] B. Fiorina, in: AIAA Scitech 2019 Forum, p. 0995.

[4] C. Fenimore, in: Symposium (International) on Combustion, volume 13, Elsevier, pp. 373–380.

[5] T. Faravelli, A. Frassoldati, E. Ranzi, Combustion and Flame 132 (2003) 188–207.

[6] A. Frassoldati, T. Faravelli, E. Ranzi, Combustion and Flame 135 (2003) 97–112.

[7] J. W. Bozzelli, A. M. Dean, International journal of chemical kinetics 27 (1995) 1097–1109.

[8] P. Glarborg, J. A. Miller, B. Ruscic, S. J. Klippenstein, Progress in Energy and Combustion Science 67 (2018) 31–68.

[9] G. P. Smith, D. M. Golden, M. Frenklach, B. Eiteener, M. Goldenberg, C. T. Bowman, R. K. Hanson, W. C. Gardiner, V. V. Lissianski, Z. W. Qin, http://www.me.berkeley.edu/gri_mech (2011).

[10] B. Fiorina, D. Veynante, S. Candel, Flow, Turbulence and Combustion 94 (2015) 3–42.

[11] P. E. Vervisch, O. Colin, J.-B. Michel, N. Darabiha, Combustion and Flame 158 (2011) 1480–1490.

[12] G. Löffler, R. Sieber, M. Harasek, H. Hofbauer, R. Hauss, J. Landauf, Industrial & engineering chemistry research 44 (2005) 6622–6633.

[13] J. Nafe, U. Maas, Proceedings of the Combustion Institute 29 (2002) 1379–1385.

[14] J. Van Oijen, L. De Goey, in: Proceedings of the European Combustion Meeting, Citeseer, pp. 1–5.

[15] G. Godel, P. Domingo, L. Vervisch, Proceedings of the Combustion Institute 32 (2009) 1555–1561.

[16] A. Vreman, B. Albrecht, J. Van Oijen, L. De Goey, R. Bastiaans, Combustion and Flame 153 (2008) 394–416.

[17] A. Ketelheun, C. Olbricht, F. Hahn, J. Janicka, Proceedings of the Combustion Institute 33 (2011) 2975–2982.

[18] F. Pecquery, V. Moureau, G. Lartigue, L. Vervisch, A. Roux, Combustion and Flame 161 (2014) 496–509.

[19] M. Ihme, H. Pitsch, Physics of Fluids 20 (2008) 055110.

[20] T. Jaravel, E. Riber, B. Cuenot, G. Bulat, Proceedings of the Combustion Institute 36 (2017) 3817–3825.

[21] M. Cailler, N. Darabiha, B. Fiorina, Submitted Combust. Flame (2018).

[22] R. Mercier, M. Cailler, B. Fiorina, in: 55th AIAA Aerospace Sciences Meeting, p. 0606.

[23] G. Maio, M. Cailler, R. Mercier, B. Fiorina, Proceedings of the Combustion Institute 37 (2019) 2591–2599.

[24] A. Cuoci, A. Frassoldati, T. Faravelli, E. Ranzi, Combustion and Flame 160 (2013) 870–886.

[25] M. Cailler, N. Darabiha, D. Veynante, B. Fiorina, Proc. Combust. Inst. (2017).

[26] www.openfoam.org, 2019.

[27] A. Cuoci, A. Frassoldati, T. Faravelli, E. Ranzi, Energy & Fuels 27 (2013) 7730–7753.

[28] A. Stagni, A. Cuoci, A. Frassoldati, T. Faravelli, E. Ranzi, Industrial & Engineering Chemistry Research 53 (2013) 9004–9016.

[29] M. S. Day, J. B. Bell, Combustion Theory and Modelling 4 (2000) 535–556.

[30] https:/github.com/acuoci/laminarSMOKE, 2019.